International Journal of Mechanical and Production Engineering Research and Development (IJMPERD)
ISSN (P): 2249-6890; ISSN (E): 2249-8001
Vol. 7, Issue 2, Apr 2017, 211-220

PREDICTION OF AERODYNAMICCHARACTERISTICS FOR SLENDER BLUFF BODIES WITH DIFFERENT NOSE CONE SHAPES

VASISHTA BHARGAVA[1] & YD DWIVEDI[2]

[1]*Department of Mechanical Engineering, GITAM University, Hyderabad, India*

[2]*Department of Aerospace Engineering, GITAM University, Hyderabad, India*

ABSTRACT

In this work, the numerical approach is used to verify the aero/hydrodynamic performance of different geometries of nose cones. Computational methods predict the flow characteristics fairly accurately in order to validate the data obtained from experiments. The simulation involves muzzle velocity that range from 5m/s to 25 m/s i.e. 1.69 to 8.4 x $10^5$and calculated for the different angle of attack, -10 to 20 degrees, to demonstrate the flow behavior around the shells. Nosecone is the most forward section of any slender moving bodies which are used in rockets, guided missiles, submarines, aircraft drop tanks and aircraft fuselage to reduce the aerodynamic or hydrodynamic drag. The basic geometry of bluff body is cylinder with variant nosecone shapes such as flat and tapered head, with moderate to low taper ratios and conical head. The aerodynamic behavior of the cylinder structures, lift, drag, and pressure distribution are illustrated for low subsonic speed. Better results are obtained for cylinder with conical head and cylinder with shapes having low and medium taper show approximately similar results.

KEYWORDS: Panel Method, Nosecone, Coefficient of Lift, Coefficient of Drag, Pressure Distribution & Angle of Attack

Received: Mar 15, 2017; **Accepted:** Mar 30, 2017; **Published:** Apr 10, 2017; **Paper Id.:** IJMPERDAPR201720

1. INTRODUCTION

The varying angles of attack aerodynamics of a symmetric body under symmetric flight conditions is problem of both academic and industry significance because the symmetric body can produce an unsymmetrical flow hence experience a side force which directly affects the aerodynamic performance and maneuverability of any flying slender body. In the past number of experimental, theoretical work were performed to understand the aerodynamic phenomena around slender bluff bodies. This topic has been reviewed by Hunt (1982) [i], Erricsson and Reding (1992) [ii] and Champigny (1994) [iii]. Allens and Perkins (1951) [iv] who studied the asymmetry in the flows that depend upon several factors such as nose shape, nose fineness ratio, length to diameter ratio, velocity, Reynolds number etc. The correlation of geometrical changes with aerodynamic performance has been studied by Levy et al (1995). The magnitude of side force is highly detrimental for the case of slender bodies with conical nose shapes Keener et al (1977) [vi]. Fidder (1985) [vii] studied about the separated flow at various incidence angles. It has been reported that the side force far exceeds the normal force for few cases Kumar and Prasad (2016) [viii]. Although the use of a conical forebody may experience a relatively lower axial force, the use of conical nose shapes is restricted due to the existence of a huge side force which is highly unpredictable Meng (2007) [ix, x]. A large amount of work has been carried out in the past few decades to identify the definitive reason for the generation of the side force over conical forebodies using experiments conducted by Jia et al (2007)

Khalid et al (1996) [xi] and Perkins et al [xii, xiii]in order to establish extent of drag force for different conical shapes. Computational work over slender body with conical nose is limited available however it is useful for validation of experimental or theoretical analysis.

In the present work, effort has been made to understand the flow field, pressure distribution around the slender body with conical nose considered sharp tip with a semi apex angle of 10 deg, flat and tapered head with moderate to low taper ratios. The slender bodies have an overall length to diameter ratio range from 0-10. Computations have been performed using numerical panel method at different angles of attack which is programmed in MATLAB software. It was concluded from previous investigations made using circular ring on an ogive shaped cylinder body had proved to reduce the side force at higher angles of attack (Ref. [vi, ix]). There has been little work done related to pressure and aerodynamic force calculation for different nosecone shapes as the flow fields change from symmetrical to unsymmetrical flow due to change of angles of attack from -10 to +20 degrees and velocity range 5-25 m/s.

2. MODEL DESCRIPTION

Four different models as shown in Figure1 cylinder A is conical with sharp tip, cylinder B with tip diameter 0.10 m, cylinder C with blunt tip diameter0.08 m and cylinder D with blunt tip diameter 0.06 m. The length of each shell is same with 0.60 m. The length to diameter ratio varied from 0 to 10. Cylinder A exhibits aerodynamic behavior as standard cone, while cylinder B, C & D with blunt tip nose exhibit behavior that resembles, to that of flat plate. It must be noted that worst case behavior is observed for cylinders (see section 4) C & D. For bluff bodies that have blunt tip or faces, the viscosity affects the boundary layer properties and hence the resulting pressure acting on the body. The flows around such body's exhibit flow separation which result in thickening of boundary layer and leaving large wake behind the body. However, no viscous effects are considered in the present study as the boundary layer interactions are complex in nature to understand the wall flows which are attached close to the surface of cylinder. Although the aerodynamic drag of cylinder A is significantly reduced in the nose tip region compared to other models it also entails the high skin friction and low pressure drag due to large wake behind the cylinder. The L/D (length to diameter) ratios of four cylinders A, B, C and D are given as (L/D) = 4.32.

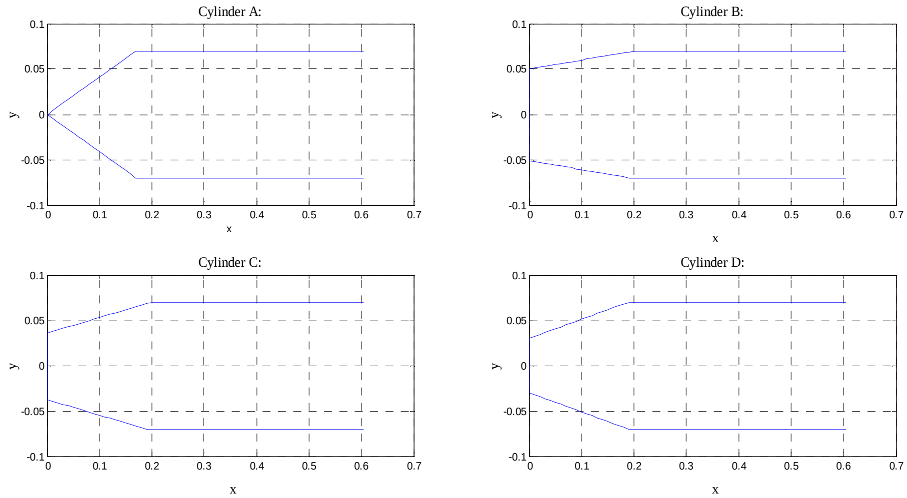


Figure 1: Geometry of different Cone Models

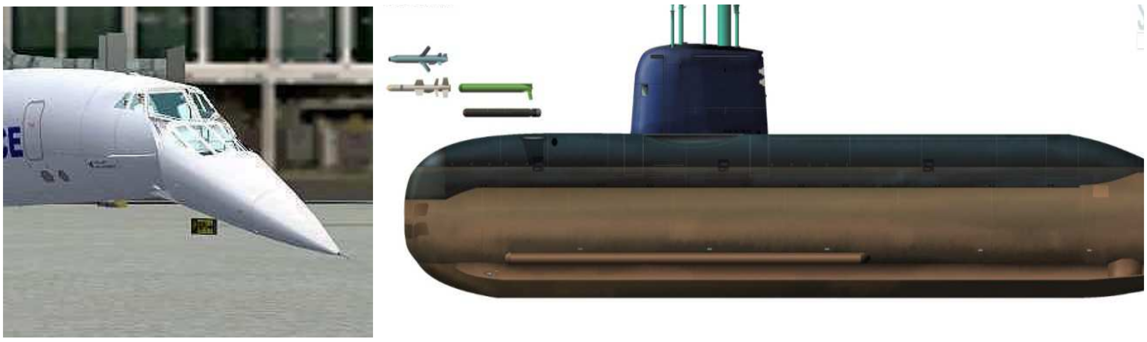


Figure 2: Nose Cone Geometry Applications

3. METHODOLOGY

A. Computational procedure

Numerical panel methods are used when computational effort required is less compared to CFD codes which solve comprehensive system of grid dependent Navier stokes equations and require extensive computational effort. Traditional methods for modeling flow around slender bodies of any shape include potential flow which utilizes the superposition of source and sink on x axis and in uniform distributed flow. However, the theory does not predict accurate values for flow whose leading edge has rounded shapes. Basic panel methods were developed by Hess and Smith at Douglas aircraft in late 1950s [v] for aircraft industry. Panel methods model the potential flow by distributing sources over the body surface. A source is point at which the fluid appears in the field at uniform rate while a sink is point which disappears at uniform rate, m^3/s. The following procedure describes the panel method calculation for 2D lifting flows

- Numbering of end points or nodes of the panels from 1…N
- The center points of each panel are chosen as *collocation points.* The boundary condition of zero flow orthogonal to surface is applied to the points.
- Panels are defined with unit normal and tangential vectors, $\hat{n}$, $\hat{t}$.
- Velocity vector, denoted by $v_{ij}$are estimated by considering the two panels, *i & j* the source on the panel *j* which induce a velocity on panel *i.* The perpendicular and tangential velocity components to the surface at the point I, are given by scalar products of $v_{ij}.\hat{n}$ and $v_{ij}.\hat{t}$
- The above quantities represent the source strength on panel j and expressed mathematically as

  $v_{ij}.\hat{n} = \sigma_j N_{ij}$

  $v_{ij}.\hat{t} = \sigma_j T_{ij}$

Where N_{ij} and $T_{ij}$are the perpendicular and tangential velocities induced at the collocation panel *i* and known as *normal and tangential influence coefficients*. The surfaces represented by the panels are solid and the following conditions are applied for the normal and tangential velocities at each of collocation points consisting of sources strengths, vortices, and oncoming velocity, U.

$$\sum_{j=1}^{N} \sigma_j N_{ij} + \gamma N_{i,N+1} + \vec{U} \cdot \hat{n}_i = v_{n_i} \tag{1}$$

$$\sum_{j=1}^{N} \sigma_j T_{t,j} + \gamma T_{t,N+1} + \vec{U} \cdot \hat{t}_i = v_{s_i} \tag{2}$$

$$\underbrace{\sum_{j=1}^{N} \sigma_j N_{ij}}_{\text{Sources}} + \underbrace{\gamma N_{i,N+1}}_{\text{Vortices}} + \underbrace{\vec{U} \cdot \hat{n}_i}_{\text{Oncoming flow}} = 0 \tag{3}$$

The above system of linear algebraic equations are solved for the N unknown source strengths, σ_i, using matrix system and expressed as

$$\mathbf{M.a = b} \tag{4}$$

Where N is an N+1 x N+1 matrix containing the N_{ij} and,σ_i is column matrix of N elements and A is the column matrix of N elements of unit normal velocity vectors. Matrix inversion procedures available in MATLAB are applied to solve for the source strengths using the above system of equations and used in the routine *foil.m* developed in MATLAB. The pressure acting at collocation point *i* is given by the Bernoulli equation as [2, 4, 5]

$$C_{pi} = 1 - \left[\frac{v_{Ti}}{U}\right]^2 \tag{5}$$

Where v_{Ti} the tangential velocity vector is determined using the influence coefficients. The influence coefficients are important for panel method in order to determine the pressure distribution over the surface of the any given airfoil coordinates

4. RESULTS AND DISCUSSIONS

A. Sharptip Nosecone Results

The pressure distribution of sharp tip nosecone (named Cylinder A) location is plotted in figure 3 for the different angles of attack ranging from -1 to +14 degrees. The plot shows that for $-1^0$and 1^0angles of attack the suction side pressure peak is highest followed by 14^0, 12^0angle of attack (AOA).The location of the pressure coefficient in axial or chord wise direction reach maximum for -1 and 1 degree AOA are same at 10 % and 20 % chord where the pressure peaks are observed due to the humps located on cylinder surface. The tangential velocity for the flow past the cylinder axis is shown in figure 4. It can be noted that the tangential velocity reached higher values for the lower surface ~ 10 &20% chord when the angle of attack is 10 deg. On the other hand the lower surface velocity is obtained for the same location i.e. 20 % chord, This change results in the pressure gradient across the cylinder length, and further The velocity contour plotted from -10 to 20 degrees AOA shows that as the AOA increases the velocity of upper surface increases and lower surface decreases. It must be noted that the computations assume the flow as non viscous in nature and operate at Reynolds number range 1.68 $x10^5$ to $8.4x10^5$. Therefore, no viscous effects and its influence on pressure drag acting on cylinder are not considered in the analysis.

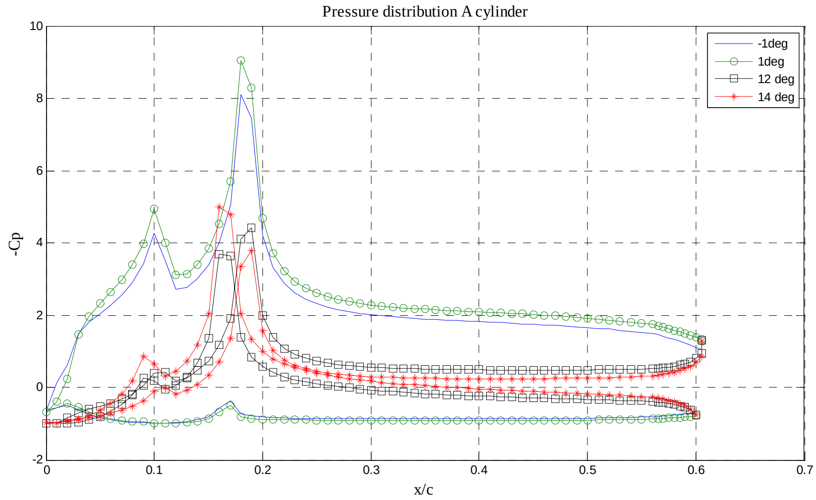


Figure 3: Pressure Distribution of Sharptip Nosecone (Cylinder A)

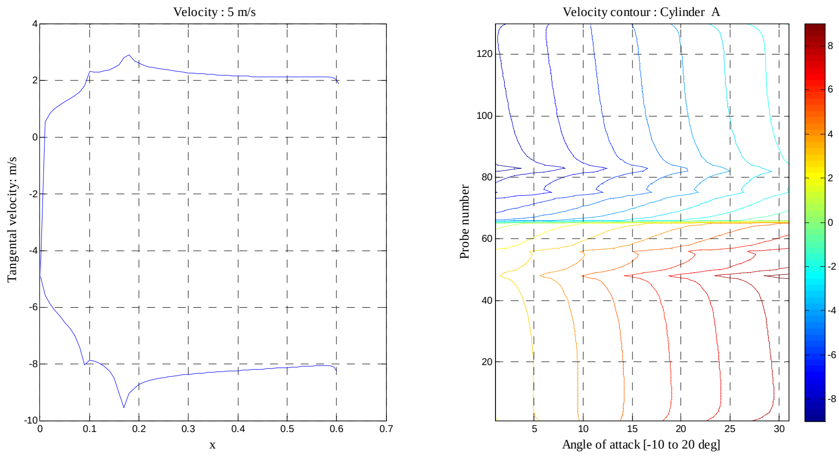


Figure 4: Tangential Velocity at 10deg AoA &Velocity Contour of Sharptip Nosecone (Cylinder A) for -10 to 20 deg AOA

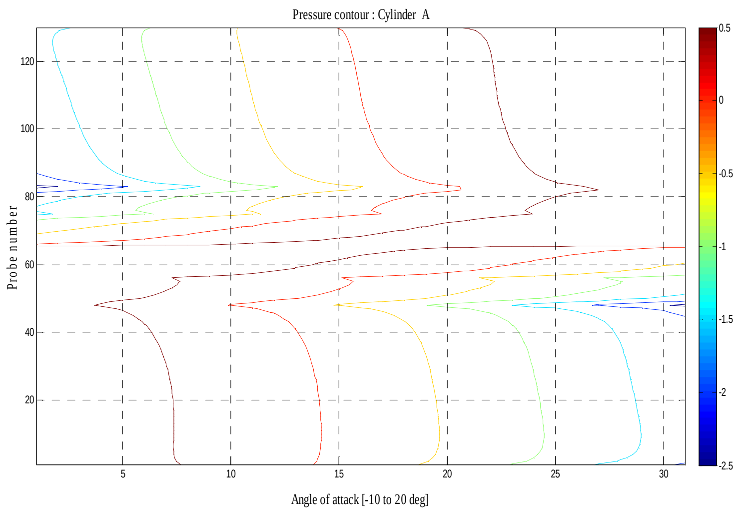


Figure 5: Pressure Contour of Sharp Nosecone (Cylinder A) for -10 to 20 deg AOA

B. Blunt Tip Nosecone Results (Cylinder B)

The pressure distribution of blunt tip nosecone (named Cylinder B), is shown in figure 5 for the different angles of attack ranging from -1 to +14 degrees. The plot shows that for 1^0 angles of attack the pressure peaks in the suction side of cylinder are identical for AoA of 12 and 14 deg. For pressure surface, there is no obvious difference in any of the configuration. The magnitude of the peak pressure coefficient along the axial direction are same as in cylinder A however, for -6^0AOA the location, there is shift in the maximum L/D ratios obtained which is observed to be different from other three configurations as shown in figure 15 (b).The velocity contour plotted (figure 6) from 0 to 30 degrees AOA shows that from 0 to 10 degrees the velocity is higher in higher in upper surface that the local flow velocity and in lower surface this is very low. Beyond 15^0 AOA, the velocities in upper and lower surfaces are negative, which shows flow reversal is likely to happen. The pressure contour figure 7 also shows that upto 10^0 AOA, the upper surface shows better pressure characteristics. Beyond 15^0 the pressure at the bottom surface is very large and flow reversal from bottom to top is expected to occur.

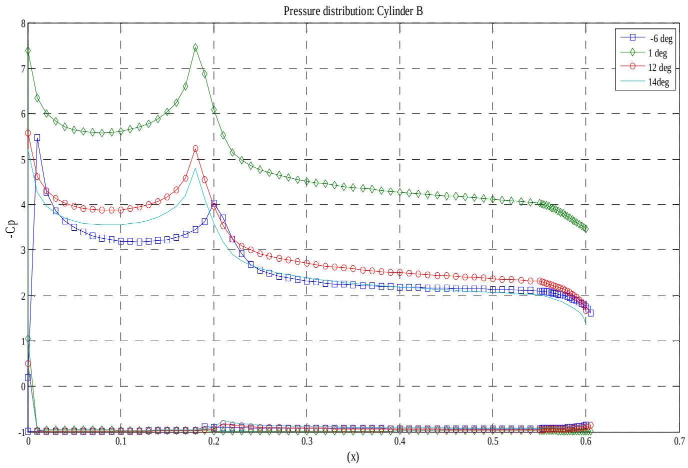


Figure 6: Pressure Distribution of Blunt Tipnosecone (Cylinder B)

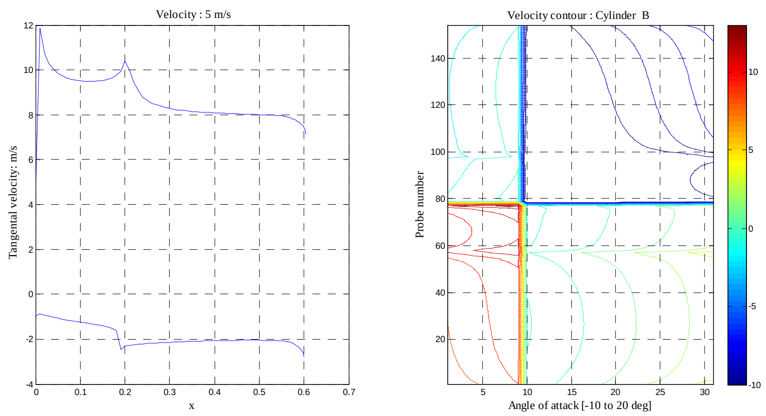


Figure 7: Velocity Contour of Blunt Tip Nosecone (Cylinder B) for -10 to 20 deg AOA

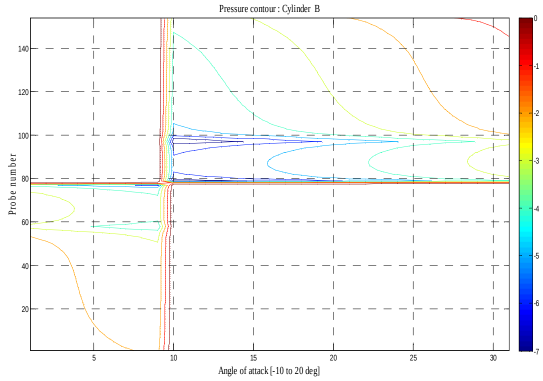


Figure 8: Pressure Contour of Blunt Tip Nosecone (Cylinder B) for -10 to 20 deg AOA

C. Blunt Tip Nosecone Results (Cylinder C& D)

The results of the medium and short tip nose cones are approximately same; the pressure coefficient at 1 degree AOA is highest in both nosecones C and D, this pertains to the point when the boundary layer thickness break and flow reversal is expected. The critical pressure coefficient for the cylinder C & D reached value of 6.5 and 4.7 as shown in figure 9a and figure 9b at 20 % chord length. However the location of the highest value is ahead in Cylinder C than D (figure 9a and 9b). The pattern of pressure coefficient for both nosecones shows small difference at the leading edge. The velocity and pressure contours of mediumtip and short tip nosecone of C and D are having almost same values (figure 10, figure 11 & figure 12). The comparison of pressure coefficient figure13 shows that the sharp tip cylinder A has high pressure peak value comparing to other three and for the Cylinder B, C and D with blunttip. This indicates that the ‘A’ is aerodynamically/hydrodynamic superior to other three configurations due to less aerodynamic drag. It must be noted that although the

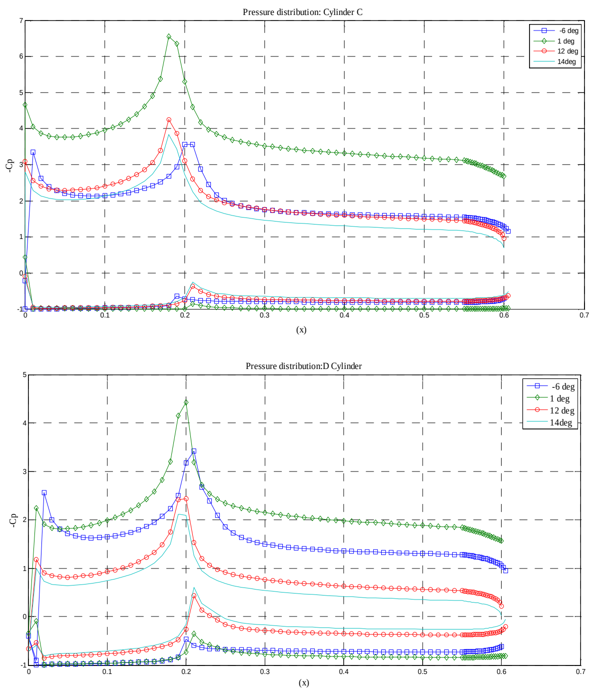


Figure 9: Pressure Distribution of Cylinder C & D Configuration at different Angle of Attack

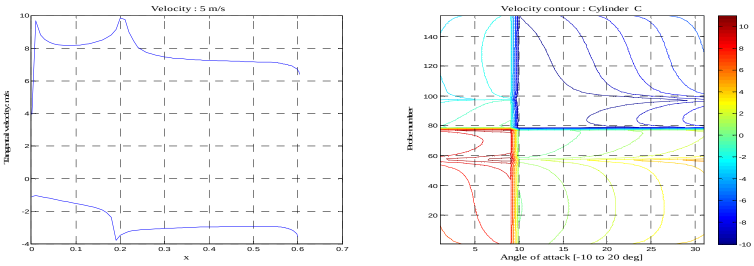


Figure 10: Velocity Contour of Medium Taper Nosecone (Cylinder C) for -10 to 20 deg AOA

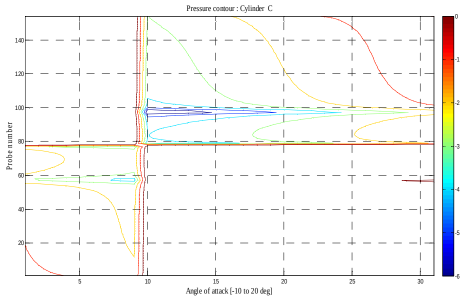


Figure 11: Pressure Contour of Medium Taper Nosecone (Cylinder C) for -10 to 20 deg AOA

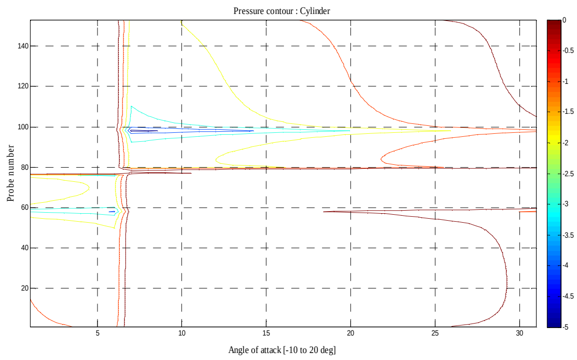


Figure 12: Pressure Contour of Short Taper Nosecone (Cylinder D).for -10 to 20 deg AOA

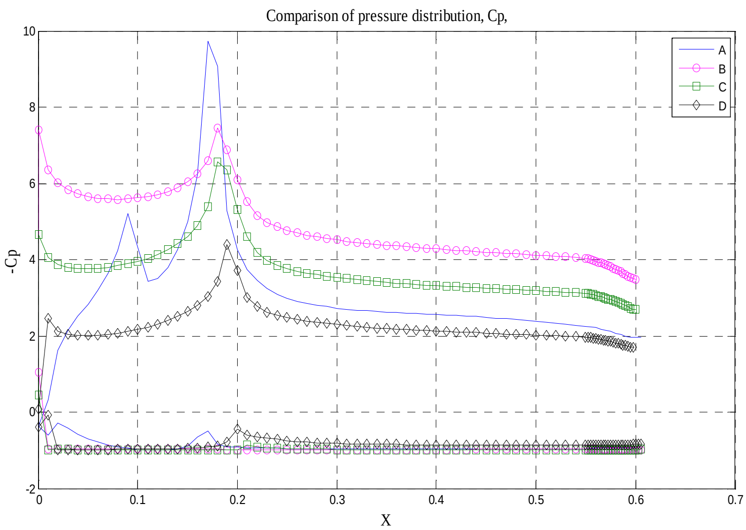


Figure 13: Comparison of Pressure Distribution of Nosecones A, B, C and D at 1 deg AOA

D. Lift & Drag Characteristics

The force coefficient such as lift and drag for four models are compared and plotted in figure 14. The value of lift and drag coefficient of sharp tip (A) is found to be the highest for all AOA followed by large tip B. The medium and short tip (C & D) has almost equal lift and drag values. The performance parameter (C_L/C_D), of the C is found to be the best followed by A. The nosecone B produce large pressure drag compared to C and D (Figure 15 & 16). The skin friction drag for model A is low due to its projection.

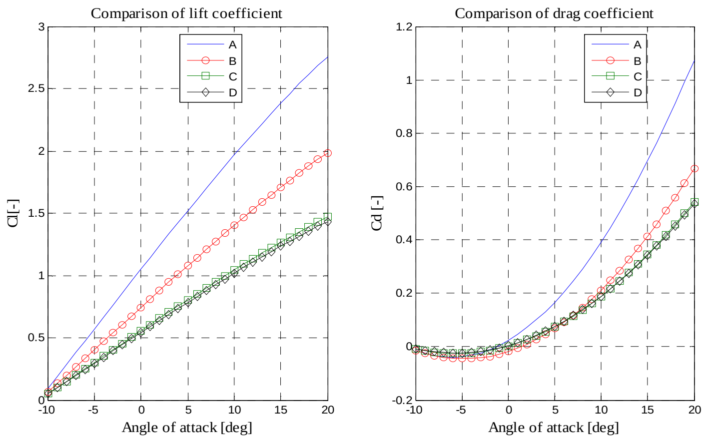


Figure 14: Coefficients of lift and Drag vs AOA for Re = 2x10^5

The cylinder B & A produce offer more side force as result of high lift force at large AoA, The flow around the nosecone for A and tapered structure for B configurations tend to generate the necessary acceleration intended during trajectory of the vehicle. However, it is accompanied with high pressure drag due to large wake behind the cylinder where the flow is fully turbulent in nature. It must be noted that flow computations do not involve viscous effects and hence results obtained do not consider the pressure drag. Although the side force developed on the cylinder models are largely dependent on the range of operating speed for a given application, it is the lift force and lift induced drag which drives the performance of the models. The other significant force acting is due to gravity which is ignored in the analysis

Figure 15 Comparison of L/D ratios and Drag polar of four Cylinder models

Figure 15 Comparison of L/D ratios and Drag polar of four Cylinder models

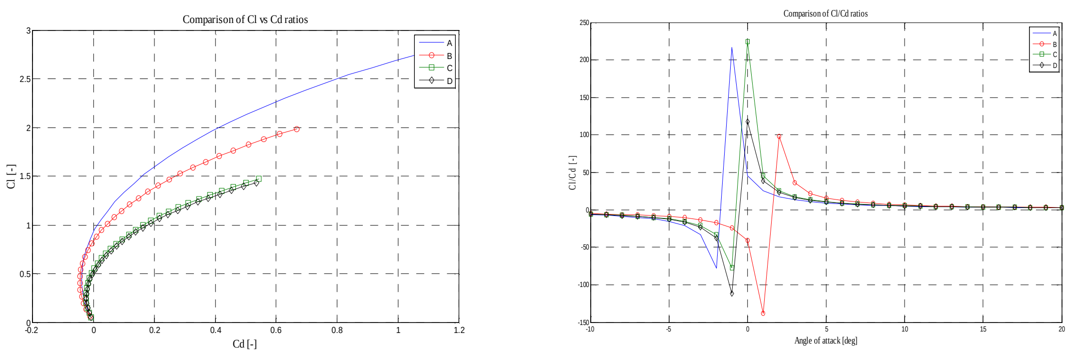


Figure 15: Comparison of L/D Ratios and Drag Polar of four Cylinder Models

5. CONCLUSIONS

The computational panel method was used to investigate the pressure, velocity and aerodynamic characteristics of

four types of nosecone due to tradeoff between the computational effort and time required. The sharptip nosecone (Cylinder A) produced high lift and high drag compared to other three configurations. The performance parameter (C_L/C_D) of medium taper (Cylinder C) is found better than other three followed by sharptip (Cylinder A) near zero degree AOA. Velocity and pressure distribution in Cylinder B and Cylinder C are almost same upto 10^0 AOA while for sharp tip nosecone the suction side pressure peak is found highest among four models. The boundary layer separation and flow reversal occurs are observed for all cylinder models which produce high pressure drag with large wakes behind. The maximum lift coefficient of 2.75 and 2 are obtained for cylinder models A & B while drag coefficient of 0.0012 for cylinders C & D. The short tip nosecone (Cylinder D) is effective only upto 6^0 AOA comparing to other which are effective upto 10^0 AOA.

6. REFERENCES

1. *Hunt, B. L., "Asymmetric Vortex Forces and Wakes on Slender Bodies," AIAA Paper, 1982-1336, Aug. 1982.*
2. *Ericsson, L., and Reding, J., "Asymmetric Flow Separation and Vortex Shedding on Bodies of Revolution," Tactical Missile Aerodynamics: General Topics, Progress in Astronautics and Aeronautics, edited by M. Hemsh, Vol. 141, New York, 1992, pp. 391–452.*
3. *Champigny, P., "Side Forces at High Angles of Attack: Why, When, How?" La Recherche Aerospatiale: Bulletin Bimestriel de l'Office National d'Etudes et de Recherches Aerospatiales, No. 4, 1994, pp. 269–282.*
4. *Allen, H.J., and Perkins, E.W., "Characteristics of Flow Over Inclined Bodies of Revolution," NACA RM-A50L07, 1951.*
5. *Haughton, Carpenter, " Aerodynamics for engineering students", Wiley eastern edition, 2001*
6. *Keener, E., Chapman, G., Cohen, L., and Taleghani, J., "Side forces on Forebodies at high angles of attack and Mach numbers from 0.1 to 0.7: two tangent ogives, paraboloid and cone," NASA TM X-3438, Feb. 1977.*
7. *Fiddes, S., "Separated Flow about Cones at Incidence–Theory and Experiment," Proceedings of Symposium on Studies of vortex Dominated Flow, NASA/LRC, 1985, pp. 285–310.*
8. *P. Kumarand J. K. Prasad, "Mechanism of Side Force Generation and Its Alleviation over a Slender Body," Journal of Spacecraft and Rockets, Vol 53, no 1, 195-208.*
9. *Jia, C., Meng, S., Qiao, Z., Gao, C., Luo, S., and Liu, F., "Pressure around a 20-degree Circular Cone at 35-degree Angle of Attack and Low Speed," AIAA Paper 2007-4453, June 2007.*
10. *Meng, X., Qiao, Z., Gao,C., Luo, S., and Liu, F., "Asymmetry Features Independent of Roll Angle for Slender Circular Cone," AIAA 2009-905, January 2009.*
11. *Khalid M. Sowoud and Rathakrishnan. E "Front Body Effects on Drag and Flow field of a Three-Dimensional Noncircular Cylinder", AIAA Journal,Vol. 31, No.7,1996,pp1345-1347.*
12. *Perkins E.W, Jorgensen L.H, and Sommer S, "Investigation of the drag of various axially symmetric nose shapes of fineness ratio 3 for Mach Numbers from 1.24 to 7.4" Report 1386 NACA, 1231-1248.*
13. *Levy Y, Hesselink L, Degani D. A Systematic Study of the Correlation between Geometrical Disturbances and Flow Asymmetry. AIAA Paper 95-0365, 1995.*